mDia and ROCK Mediate Actin-Dependent Presynaptic Remodeling Regulating Synaptic Efficacy and Anxiety

AUTHOR(S):

Deguchi, Yuichi; Harada, Masaya; Shinohara, Ryota; Lazarus, Michael; Cherasse, Yoan; Urade, Yoshihiro; Yamada, Daisuke; ... Watanabe, Dai; Furuyashiki, Tomoyuki; Narumiya, Shuh

CITATION:

Deguchi, Yuichi ...[et al]. mDia and ROCK Mediate Actin-Dependent Presynaptic Remodeling Regulating Synaptic Efficacy and Anxiety. Cell Reports 2016, 17(9): 2405-2417

ISSUE DATE:

2016-11-22

URL:

http://hdl.handle.net/2433/217361

Article

Cell Reports

mDia and ROCK Mediate Actin-Dependent Presynaptic Remodeling Regulating Synaptic Efficacy and Anxiety

Graphical Abstract

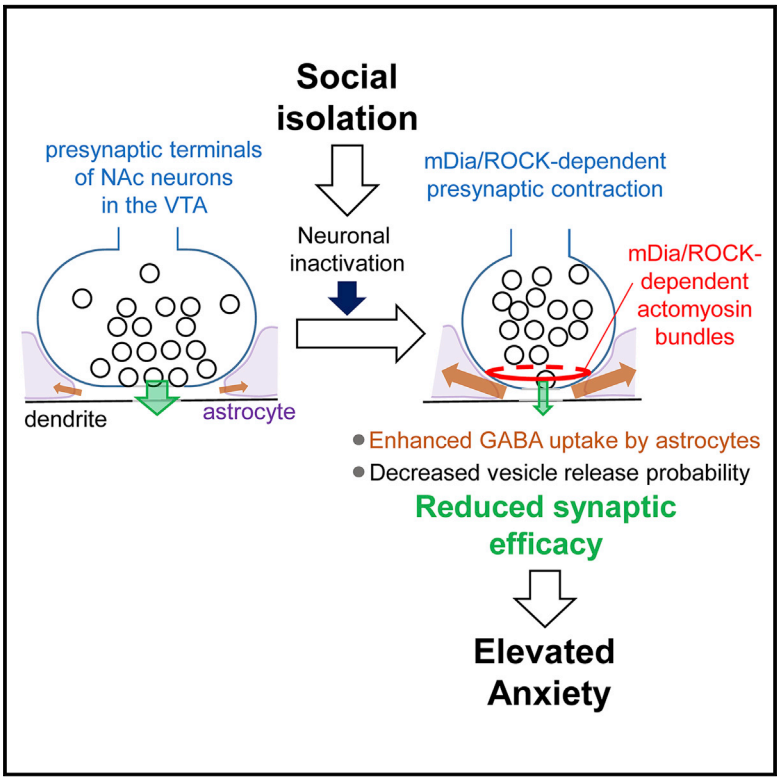

Authors

Yuichi Deguchi, Masaya Harada, Ryota Shinohara, ..., Dai Watanabe, Tomoyuki Furuyashiki, Shuh Narumiya

Correspondence

y-deguchi@nagasaki-u.ac.jp (Y.D.), snaru@mfour.med.kyoto-u.ac.jp (S.N.)

In Brief

Little is known about how experiences cause morphological and functional changes in presynaptic terminals to affect behaviors. Deguchi et al. show that social isolation elevates anxiety-like behavior through contraction of presynaptic terminals, thereby reducing synaptic efficacy of NAc neurons. The effect is mediated by mDia, an actin nucleator, and ROCK.

Highlights

- Social-isolation-induced anxiety requires mDia, an actin nucleator, in NAc neurons
- mDia induces actin filaments around edges of the synaptic cleft in presynaptic terminals
- mDia- and ROCK-dependent actomyosin in presynaptic terminals induces contraction
- mDia-mediated presynaptic contraction reduces GABAergic synaptic efficacy for anxiety

Deguchi et al., 2016, Cell Reports *17*, 2405–2417
November 22, 2016
http://dx.doi.org/10.1016/j.celrep.2016.10.088

CellPress

Cell Reports
Article

mDia and ROCK Mediate Actin-Dependent Presynaptic Remodeling Regulating Synaptic Efficacy and Anxiety

Yuichi Deguchi,[1,*] Masaya Harada,[1] Ryota Shinohara,[1] Michael Lazarus,[2] Yoan Cherasse,[2] Yoshihiro Urade,[2] Daisuke Yamada,[3] Masayuki Sekiguchi,[3] Dai Watanabe,[4] Tomoyuki Furuyashiki,[1] and Shuh Narumiya[1,5,*]
[1]Medical Innovation Center, Kyoto University Graduate School of Medicine, Kyoto 606-8507, Japan
[2]International Institute for Integrative Sleep Medicine, University of Tsukuba, Ibaraki 305-8575, Japan
[3]Department of Degenerative Neurological Diseases, National Institute of Neuroscience, National Center of Neurology and Psychiatry, Tokyo 187-8502, Japan
[4]Department of Biological Sciences, Kyoto University Graduate School of Medicine, Kyoto 606-8501, Japan
[5]Lead Contact
*Correspondence: y-deguchi@nagasaki-u.ac.jp (Y.D.), snaru@mfour.med.kyoto-u.ac.jp (S.N.)
http://dx.doi.org/10.1016/j.celrep.2016.10.088

SUMMARY

Here, we show neuronal inactivation-induced presynaptic remodeling and involvement of the mammalian homolog of Diaphanous (mDia) and Rho-associated coiled-coil-containing kinase (ROCK), Rho-regulated modulators of actin and myosin, in this process. We find that social isolation induces inactivation of nucleus accumbens (NAc) neurons associated with elevated anxiety-like behavior, and that mDia in NAc neurons is essential in this process. Upon inactivation of cultured neurons, mDia induces circumferential actin filaments around the edge of the synaptic cleft, which contract the presynaptic terminals in a ROCK-dependent manner. Social isolation induces similar mDia-dependent presynaptic contraction at GABAergic synapses from NAc neurons in the ventral tegmental area (VTA) associated with reduced synaptic efficacy. Optogenetic stimulation of NAc neurons rescues the anxiety phenotype, and injection of a specific ROCK inhibitor, Y-27632, into the VTA reverses both presynaptic contraction and the behavioral phenotype. mDia-ROCK signaling thus mediates actin-dependent presynaptic remodeling in inactivated NAc neurons, which underlies synaptic plasticity in emotional behavioral responses.

INTRODUCTION

Whether structural remodeling of synapses underlies synaptic and behavioral plasticity has been a fundamental question in neuroscience (Caroni et al., 2012). Long-term potentiation or depression of synaptic efficacy is accompanied by enlargement or shrinkage of dendritic spines, respectively (Bosch and Hayashi, 2012), and dendritic spine formation occurs in pertinent cortical structures during behavioral learning in a manner correlated to behavioral performance (Xu et al., 2009), thus supporting a critical role of morphological changes of postsynaptic structure in synaptic and behavioral plasticity. In contrast, presynaptic remodeling in the adult brain for synaptic and behavioral plasticity remains to be elucidated.

The actin cytoskeleton plays a critical role in morphogenesis of dendritic spines, and a role of Rho guanosine-5'-triphosphate (GTPases), regulators of actin reorganization (Hall and Nobes, 2000), in this remodeling has been well characterized (Tolias et al., 2011). In mice, reduction of Rac1 signaling in nucleus accumbens (NAc) neurons increased stubby dendritic spines and induced depression-related behaviors after chronic social defeat stress (Golden et al., 2013). Mice deficient in effector molecules of Rho GTPases, such as cofilin and Arp2/3, showed loss or abnormal morphology of dendritic spines and impaired learning and emotional behaviors (De Filippis et al., 2014). In contrast, little is known about the roles of actin cytoskeleton and Rho GTPases in the presynapse, although they are possibly involved in synaptic vesicle release, recycling, and replenishment (Morales et al., 2000; Sankaranarayanan et al., 2003; Watanabe et al., 2013; Bleckert et al., 2012). Pilo Boyl et al. (2007) reported that profilin 2 regulates presynaptic actin polymerization and vesicle exocytosis, which is related to novelty-seeking behavior.

Among Rho GTPases, Rho regulates actomyosin formation through mammalian homolog of Diaphanous (mDia) and Rho-associated coiled-coil-containing kinase (ROCK) (Narumiya et al., 2009). mDia promotes actin nucleation and polymerization (Watanabe et al., 1997). ROCK activates myosin light chain and cooperates with mDia to form actomyosin bundles and generate contractility (Narumiya et al., 2009). In *Drosophila*, Diaphanous, an mDia ortholog, modulates actin and microtubule cytoskeletons in nerve terminals at the neuromuscular junction (Pawson et al., 2008). There are three mDia isoforms, mDia1–3, in mammals, among which mDia1 and mDia3 are expressed in the mouse brain during and after development (Shinohara et al., 2012). Given functional redundancy of mDia1 and mDia3, we generated a double-knockout mouse lacking both mDia1 and mDia3 and found several abnormalities during brain development (Thumkeo et al.,

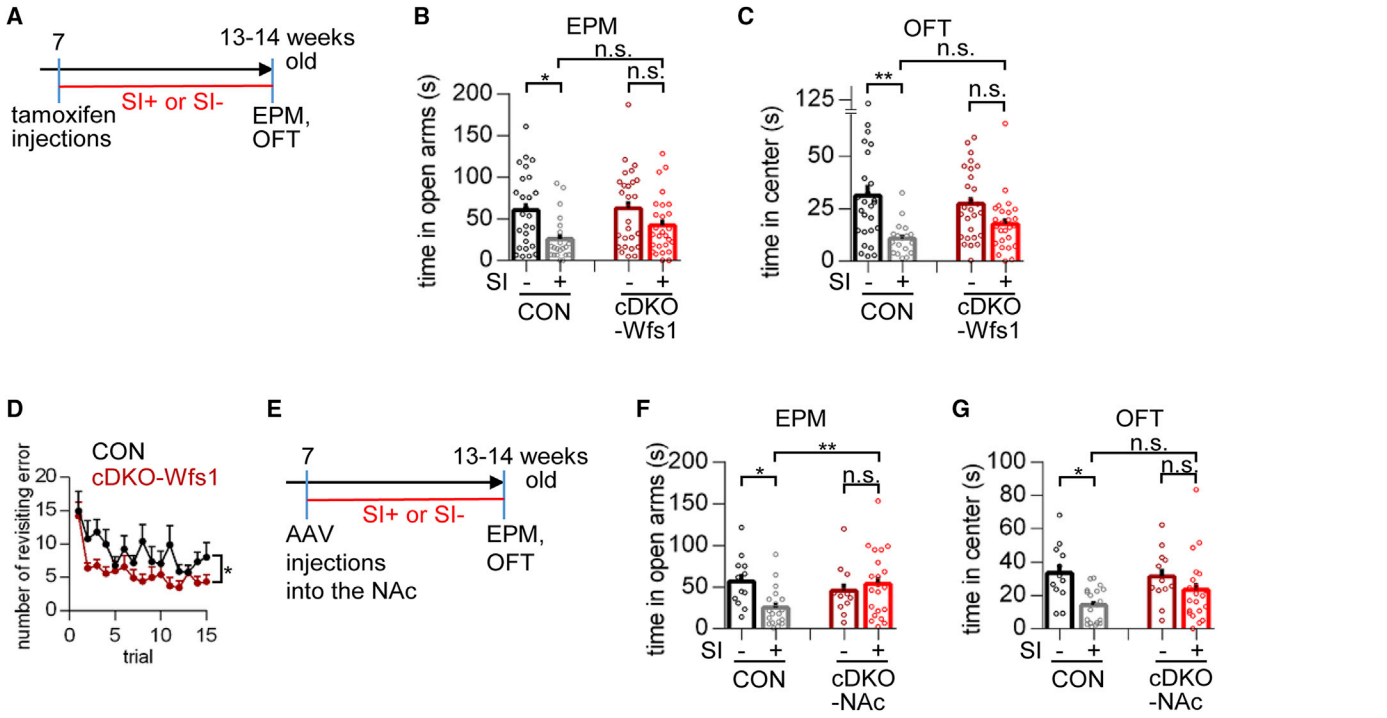

Figure 1. mDia in NAc Neurons Mediates Social-Isolation-Induced Elevated Anxiety

(A) Schedules of social isolation (SI). All mice were injected with tamoxifen at 7 weeks old. One group was subjected to social isolation (SI^+) and the other was kept in groups (SI^-) from 7 to 13–14 weeks old.

(B and C) Time in open arm in EPM (B) and in the center in OFT (C) of control (CON) and mDia-cDKO-Wfs mice with or without social isolation. n = 18–27 mice for each group. *$p < 0.05$, **$p < 0.01$, and not significant (n.s.), Bonferroni post hoc test following two-way ANOVA. Data are shown as mean ± SEM.

(D) Radial maze test of CON and mDia-cDKO-Wfs1 mice (n = 13 and 16, respectively). *$p < 0.05$ between the two groups in repeated-measures two-way ANOVA. Data are shown as mean ± SEM.

(E) Protocol of AAV injection and SI.

(F and G) Time in open arm in EPM (F) and in the center in OFT (G). n = 12–21 mice for each group. *$p < 0.05$, **$p < 0.01$, and not significant (n.s.), Bonferroni post hoc test following two-way ANOVA. Data are shown as mean ± SEM.

See also Figures S1 and S2.

2011; Shinohara et al., 2012), which precluded further analyses of mDia functions in the adult brain. To circumvent this problem and investigate functions of mDia in neuronal and behavioral plasticity in adult mice, we have conditionally deleted mDia1 and mDia3 in the nucleus accumbens (NAc) after brain maturation and subjected these mice to social isolation. Our analysis has revealed that social isolation induces presynaptic remodeling in NAc neurons projecting to the ventral tegmental area (VTA) in a manner dependent on mDia and ROCK, which reduces synaptic efficacy and underlies social-isolation-induced elevated anxiety. Our study thus demonstrates a role of mDia- and ROCK-dependent presynaptic remodeling in synaptic and behavioral plasticity.

RESULTS

mDia in the Adult Brain Is Involved in Regulation of Behaviors

To analyze mDia functions in the adult brain, we generated *mDia1/3* double floxed mice (mDiaDF) and bred them with Wfs1-Tg3-CreERT2 mice, which express tamoxifen-inducible Cre selectively in NAc neurons, CA1 pyramidal cells in the hippocampus, and layer II/III cortical neurons (Madisen et al., 2012) (Figures S1A and S1B). We used the resultant offspring with or without the hemizygous *Cre* allele as mDia1 and mDia3 conditional double-knockout mice (mDia-cDKO-Wfs1) or littermate controls, respectively. mDia-cDKO-Wfs1 mice indeed exhibited marked decrease in *mDia3* mRNA expression in the NAc (Figure S1C). Using these mice, we examined a role of mDia in behavioral changes induced by chronic stress, either social isolation or social defeat. Whereas prolonged social isolation increased anxiety-like behaviors in the elevated plus maze test (EPM) and the open-field test (OFT) in control mice, these isolation-induced changes were attenuated in mDia-cDKO-Wfs1 mice (Figures 1A–1C). After social isolation, the number of mDia-cDKO-Wfs1 mice that showed anxiety-like behaviors beyond defined thresholds in both tests was significantly fewer than that of control mice (Figure S1D). In contrast, repeated social defeat stress induced social avoidance and anxiety-like behavior similarly in mDia-cDKO-Wfs1 mice and littermate controls (Figures S1E–S1G). These results suggest that mDia1 and mDia3 in the adult brain critically contribute to induction of anxiety-like behaviors by prolonged social isolation.

mDia-cDKO-Wfs1 mice were normal in most behavioral tests (Figures S1H–S1N), except improved performance in the radial

maze test, a test for working memory driven by food reward (Figure 1D). However, they appeared normal in the Y maze test (Figure S1O), another working memory test based on innate alternating behavior, suggesting that mDia may regulate working memory context dependently.

mDia in NAc Neurons Is Critical for Isolation-Induced Elevated Anxiety

To pinpoint the above-mentioned actions of mDia1 and mDia3 to those in NAc neurons, we used adeno-associated virus (AAV) serotype rh10 expressing Cre (AAV-Cre), which reduced the expression of mDia1 and mDia3 to the negligible level by 7 days after infection in mDiaDF primary cultured neurons (Figure S2A). We injected AAV-Cre together with AAV-mCherry into the NAc of mDiaDF mice to delete mDia 1 and mDia3 specifically in NAc neurons (mDia-cDKO-NAc) (Figures S2B and S2C). These mDia-cDKO-NAc mice failed to show social-isolation-induced elevated anxiety-like behaviors both in EPM and OFT, whereas control mice that received AAV-mCherry alone showed such behaviors as before (Figures 1E–1G). These results show that mDia1 and mDia3 in NAc neurons are thus critical for elevated anxiety induced by social isolation. To examine further the role of mDia action in NAc neurons, we applied behavioral sensitization by repeated cocaine exposure, which potentiates GABAergic synapse from NAc neurons to VTA neurons and disinhibits dopamine neurons (Bocklisch et al., 2013), to these mice after social isolation. Social isolation blunted sensitization to repeated cocaine exposure in wild-type mice, but not in mDia-cDKO-NAc mice (Figure S2D), suggesting that mDia in NAc neurons possibly regulates synaptic transmission in projection of NAc to VTA neurons.

Social-isolation-induced anxiety-like behaviors were reported due to decreased excitability of neurons in the NAc (Wallace et al., 2009). Indeed, social isolation reduced phosphorylation of cAMP response element binding protein (pCREB) in NAc neurons in control mice as reported. However, social isolation did not affect the pCREB level in NAc neurons of mDia-cDKO-Wfs1 mice (Figures S2E and S2F). Notably, in mDia-cDKO-NAc mice, the pCREB level was intact not only in AAV-mCherry-infected mDia-deficient neurons but also in populations of NAc neurons without mCherry expression within and at the periphery of the AAV-mCherry-infected area (Figures S2G and S2H). These findings show that the loss of mDia in NAc neurons can attenuate CREB phosphorylation in the surrounding mDia-intact NAc neurons and indicate that mDia in NAc neurons regulates isolation-induced reduction of CREB phosphorylation indirectly in a non-cell-autonomous manner (Figures S2G and S2H).

Neuronal Inactivation Induces mDia Recruitment at Presynaptic Terminals

To obtain an insight into mDia actions in neurons, we prepared the primary culture of hippocampal neurons and examined the subcellular localization of mDia at 15–21 days in vitro (DIV). Because of the lack of suitable antibodies to mDia1 or mDia3 for immunofluorescence, we infected neurons with AAV expressing EGFP-fused mDia1 or mDia3 to visualize mDia localization. Under the basal conditions, EGFP-mDia1 and EGFP-mDia3 were distributed mostly in axons and somatodendritic regions uniformly and only occasionally accumulated in the presynaptic terminals. We then investigated whether neuronal activity affects mDia localization. We treated cultured neurons with tetrodotoxin (TTX) for neuronal inactivation. TTX at 10 nM quickly reduced spontaneous postsynaptic currents and action potentials (Figure 2A), and decreased pCREB level at 24 hr (Figures 2B and S3A). Concomitantly, EGFP-mDia1 and EGFP-mDia3 accumulated in both synapsin1/2-positive, putative glutamatergic (Figures 2C, 2D, S3B, and S3C) and vesicular gamma-Aminobutyric acid (GABA) transporter (VGAT)-positive, putative GABAergic presynaptic terminals (Figures 2E and S3D). Although some presynaptic terminals were negative for EGFP-mDia accumulation after TTX treatment, they were apparently derived from non-infected neurons, because EGFP-mDia3-positive presynaptic terminals were always accompanied by expression of simultaneously transfected synaptophysin-mCherry, and the proportion of $EGFP^+mCherry^+$ neurons is the same as that of $EGFP^+$ $mCherry^+$ presynaptic terminals (Figure S3E). Notably, TTX treatment for 24 hr did not induce accumulation of soluble EGFP to the presynaptic terminals (Figure S3F), indicating that TTX-induced presynaptic accumulation of EGFP-mDia1/3 is not due to pH or volume effects. We also examined whether accumulation of EGFP-mDia also occurs at postsynaptic structures in TTX-treated neurons. We visualized dendritic spines with an actin filament probe, the calponin homology domain of utrophin fused to mCherry (mCherry-UtrCH) (Burkel et al., 2007), which exhibited the same signal pattern as phalloidin in cultured neurons (Figure S3G) and were enriched at dendritic spines. Using this probe, we found that EGFP-mDia3 was evenly distributed in dendritic spines and shafts before and after TTX treatment (Figures S3H and S3I). We next treated cultured neurons with 4-aminopyridine (4-AP) for 2 hr to increase neuronal activity. Treatment with 4-AP increased CREB phosphorylation and c-Fos expression (Figure S3J), but did not induce apparent changes in EGFP-mDia3 localization (Figure 2C). Collectively, these findings suggest that mDia1 and mDia3 are recruited specifically to presynaptic terminals upon neuronal inactivation.

mDia Mediates Inactivation-Induced Formation of Actin Filaments at the Edges of Synaptic Clefts in Presynaptic Terminals

Given the actin polymerization activity of mDia, we next wondered whether mDia accumulation upon neuronal inactivation leads to actin filament formation in presynaptic terminals. To this aim, we sparsely infected primary mDiaDF neurons with AAV expressing mCherry-UtrCH from 7 DIV, and examined mCherry-UtrCH signals at 15–21 DIV by silver-enhanced immunogold electron microscopy. This method enabled us to examine the distribution of actin filaments in presynaptic terminals in the presence of dendritic spines of much higher actin filament density (Figure S4A). We deleted mDia by simultaneous infection with AAV-Cre (mDia-cDKO-AAV). Immunoelectron microscopy revealed TTX-induced alteration in mCherry-UtrCH distribution within presynaptic terminals despite similar mCherry-UtrCH intensity at presynaptic terminals in control and TTX-treated neurons detected by light microscopy (Figure S4B). We first investigated symmetric, putative GABAergic synapses attached to the dendritic shaft with the synaptic cleft, along which the membrane

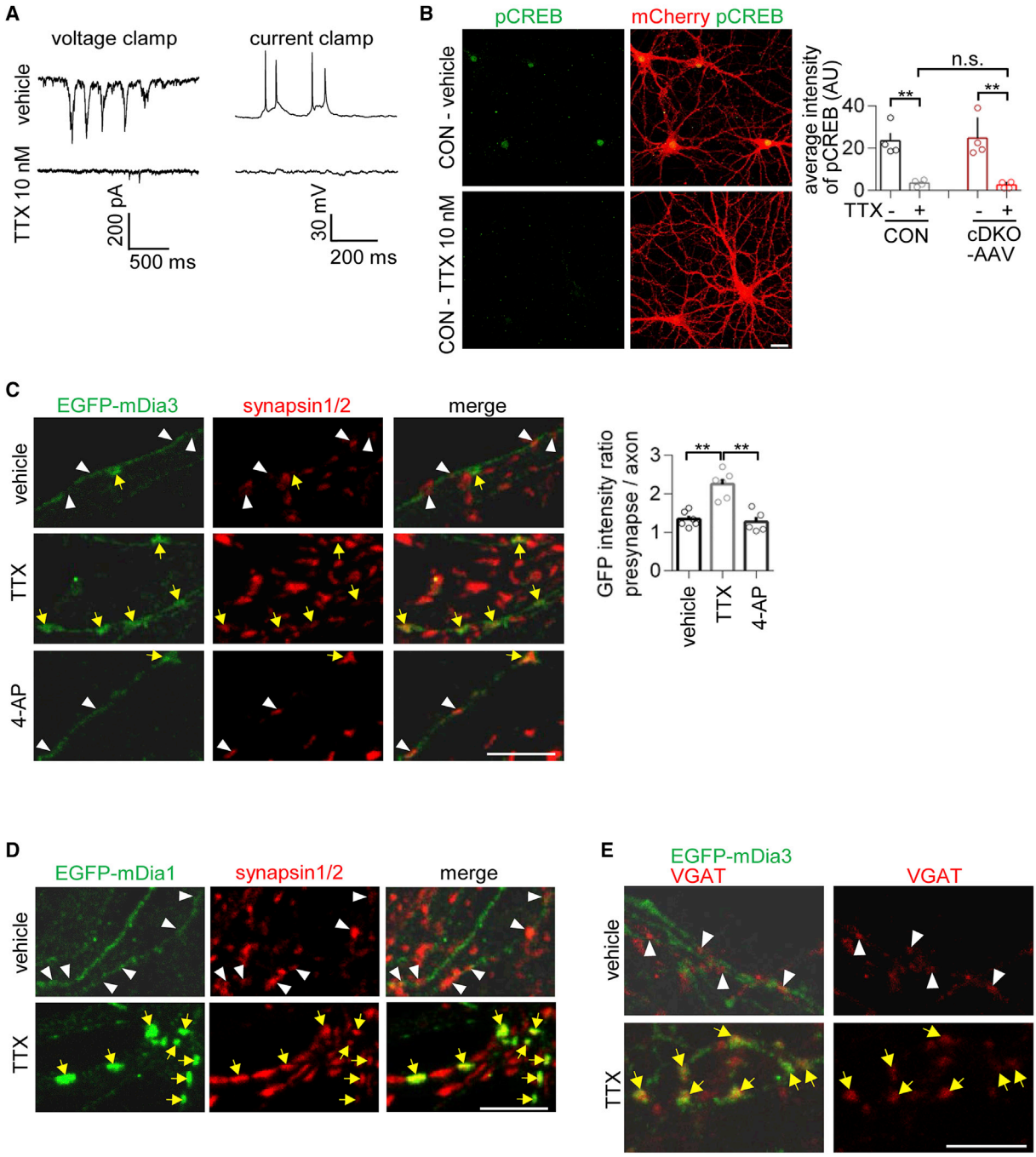

Figure 2. Neuronal Inactivation Recruits mDia1 and mDia3 to Presynaptic Terminals in Cultured Neurons

(A and B) TTX-induced suppression of spontaneous firing (A) and CREB phosphorylation (B) of cultured neurons. (B) Representative immunofluorescence images of control (CON) and mDia-deficient neurons (cDKO-AAV) treated with vehicle or 10 nM TTX for 24 hr (left) and the averaged fluorescence intensities for pCREB in neurons in each culture are shown (right). Scale bar, 40 μm. Four independent cultures were used in each group, and 25–30 neurons were examined in each culture. **$p < 0.01$ and not significant (n.s.), Bonferroni post hoc test following two-way ANOVA. (B) Data are shown as mean ± SEM.

(C) Immunofluorescence analysis for EGFP-mDia3 distribution in 21 DIV neurons treated with vehicle, TTX, or 4-AP. Representative images (left) and the ratio of fluorescence intensity for EGFP in presynaptic terminals to axonal segments are shown (right). The regions defined as presynaptic terminals and axonal segments for quantification are shown in Figure S3B. n = 5–6 independent cultures treated with vehicle, TTX, and 4-AP, respectively. **$p < 0.01$, Bonferroni post hoc test following one-way ANOVA. Scale bar, 5 μm. Data are shown as mean ± SEM.

(legend continued on next page)

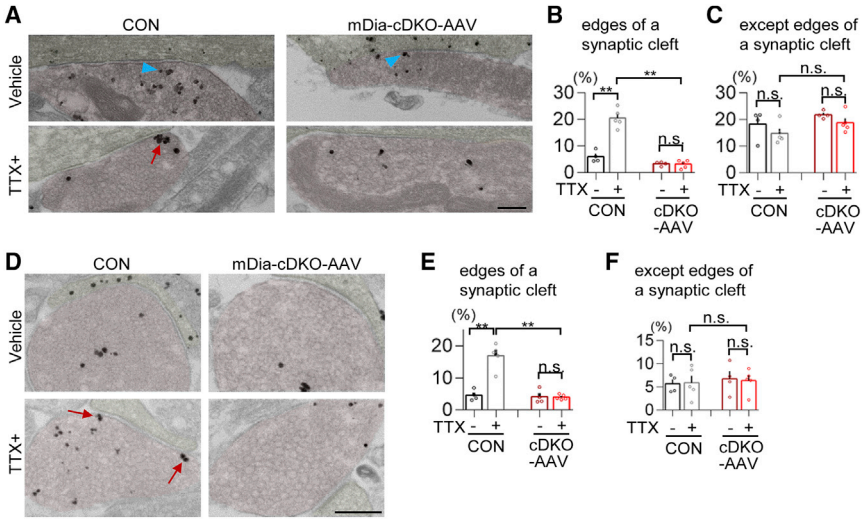

Figure 3. Inactivation-Induced, mDia-Dependent Actin Filament Formation at Edges of Synaptic Clefts in Presynaptic Terminals in Cultured Neurons

(A and D) Representative images of silver-enhanced immunogold electron microscopy for mCherry-UtrCH at symmetric (A) and asymmetric synapses (D). Presynaptic or postsynaptic structures are colored in pale red or yellow, respectively. Scale bars, 200 nm.

(B, C, E, and F) Percent deposition of mCherry-UtrCH signals in the presynaptic edge and the presynaptic submembrane out of total signals in the presynaptic terminal of symmetric synapses (B and C) and asymmetric synapse (E and F). The presynaptic edge and the presynaptic submembrane are defined in Figure S4C, and signals in each are indicated by red arrows and blue arrowheads (A and D). n = 4–5 independent cultures (B and C: 8–16 synapses per culture; E and F: 9–16 synapses per culture) for respective groups. **$p < 0.01$ and not significant (n.s.), Bonferroni post hoc test following two-way ANOVA. Data are shown as mean ± SEM. See also Figure S4.

domain with the postsynaptic density (PSD) and its surrounding regions were found (Figure S4C). TTX treatment for 24 hr enriched mCherry-UtrCH signals at the edges of synaptic clefts in these presynaptic GABAergic terminals of control neurons, whereas such enrichment was absent in mDia-cDKO-AAV neurons (Figures 3A, 3B, and S4D). On the other hand, mCherry-UtrCH signals along the synaptic cleft 100 nm outside from the edge were similarly distributed in mDia-cDKO-AAV and control neurons (Figure 3C). Furthermore, the total numbers of mCherry-UtrCH signals in each presynaptic terminal were not altered by mDia-deficiency or the TTX treatment (Figure S4E). A similar mDia-dependent enrichment of mCherry-UtrCH signals was also seen for asymmetric, putative excitatory synapses (Figures 3D–3F and S4F). These results suggest that prolonged neuronal inactivation induces actin filament formation at the edges of synaptic clefts in presynaptic terminals of both inhibitory and excitatory synapses in an mDia-dependent manner.

mDia Cooperates with ROCK for Inactivation-Induced Presynaptic Contraction

We then examined morphological change of presynaptic terminals upon neuronal inactivation by electron microscopy. Under the basal condition, the length of synaptic clefts was not significantly different between control AAV-mCherry-infected mDiaDF neurons and mDia-cDKO-AAV neurons (Figures 4A, 4B, and S5A). TTX treatment for 24 hr shortened the length of synaptic clefts of symmetric synapses in control neurons, but not that in mDia-cDKO-AAV neurons (Figures 4A, 4B, and S5A). The TTX treatment also decreased the number of mitochondria in presynaptic terminals of control neurons, but not mDia-cDKO-AAV neurons, whereas the numbers of dense core vesicles and synaptic vesicles in the presynaptic terminal were not different between control and mDia-cDKO-AAV neurons (Figure S5B). mDia cooperates with another Rho effector, ROCK, to form actomyosin bundles upon Rho activation. We therefore added either Y-27632, a ROCK inhibitor, or blebbistatin, a myosin II inhibitor, to control neurons together with TTX. The length of synaptic clefts at symmetric synapses was significantly longer with Y-27632 or blebbistatin treatment than respective vehicle treatment (Figures 4C–4E, S5C, and S5D). By contrast, TTX, Y-27632, blebbistatin, and mDia deficiency did not affect the length of PSD at symmetric synapses (Figures 4F, S5E, and S5F). These findings suggest that mDia and ROCK cooperate together to form circumferential actomyosin bundles at the edge of the synaptic cleft and induce presynaptic contraction upon neuronal inactivation.

We then analyzed effects of TTX-induced presynaptic contraction by whole-cell patch-clamp recording. Whereas TTX treatment for 24 hr decreased amplitudes of miniature inhibitory postsynaptic currents (mIPSCs) in the control neurons, the mIPSC amplitudes in mDia-deficient neurons were not affected by the TTX treatment and were significantly larger than those in TTX-treated control neurons (Figures 4G and 4H). On the other hand, the mIPSC frequency varied considerably (Figure S5G), perhaps because of a large variability in the number of inhibitory synapses across neurons (Figure S5H), which precluded detailed analyses on this parameter. These findings suggest that prolonged neuronal inactivation induces presynaptic contraction, leading to decreased response of GABAergic synapses in an mDia-dependent manner.

(D and E) Immunofluorescence analysis for EGFP-mDia1 and synapsin1/2 (D) and EGFP-mDia3 and VGAT (E) distribution in cultured neurons treated with vehicle or TTX. Scale bars, 5 μm.

(C–E) Yellow arrows or white arrowheads indicate presynaptic terminals with or without EGFP-mDia recruitment, respectively.

See also Figure S3.

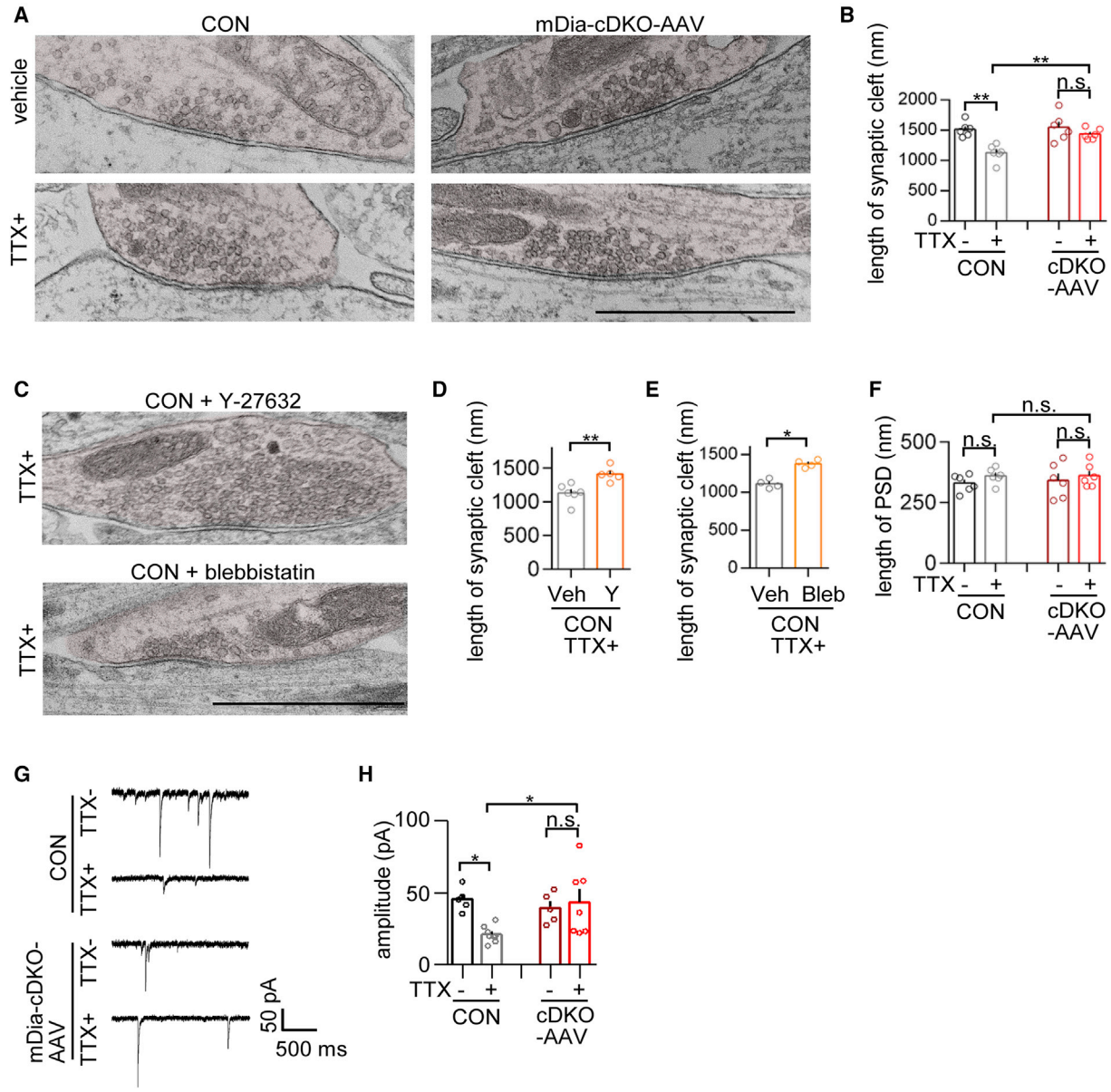

Figure 4. Inactivation-Induced, mDia-Dependent Contraction of GABAergic Presynaptic Terminals and Altered Postsynaptic Response in Cultured Neurons

(A and B) Representative electron micrographs (A) and the synaptic cleft length (B) of symmetric synapses of control (CON) and mDia-cDKO-AAV neurons treated with vehicle or TTX. (A) Presynaptic structures are colored in pale red. Scale bar, 1 μm. (B) Only the synapses with PSD longer than 200 nm were analyzed. n = 6 independent cultures (9–22 synapses per culture) for each group. *$p < 0.05$, **$p < 0.01$, and not significant (n.s.), Bonferroni post hoc test following two-way ANOVA. (B) Data are shown as mean ± SEM.

(C–E) Representative electron micrographs (C) and the synaptic cleft length (D and E) of symmetric synapses of TTX-treated mDia-intact neurons simultaneously treated with Y-27632 or blebbistatin. Scale bar, 1 μm. The values of TTX-treated, vehicle-controlled neurons in (D) were taken from those shown in (B). Only symmetric synapses with PSD longer than 200 nm were analyzed. n = 6 and 5 (D) or n = 4 and 4 (E) independent cultures (9–27 synapses per culture) for respective groups. *$p < 0.05$ and **$p < 0.01$, Mann-Whitney test. (D and E) Data are shown as mean ± SEM.

(F) The length of PSD of symmetric synapses. The same sets of synapses in (B) were analyzed. n = 6 independent cultures (9–22 synapses per culture) for each group. p value is not significant (n.s.), Bonferroni post hoc test following two-way ANOVA. Data are shown as mean ± SEM.

(G and H) Representative traces (G) and amplitudes (H) of mIPSCs of control (CON) and mDia-cDKO-AAV neurons with or without TTX treatment. n = 5–8 neurons for each group (H). One or two neurons were recorded from a single culture. *$p < 0.05$, **$p < 0.01$, and not significant (n.s.), Bonferroni post hoc test following two-way ANOVA.

See also Figure S5.

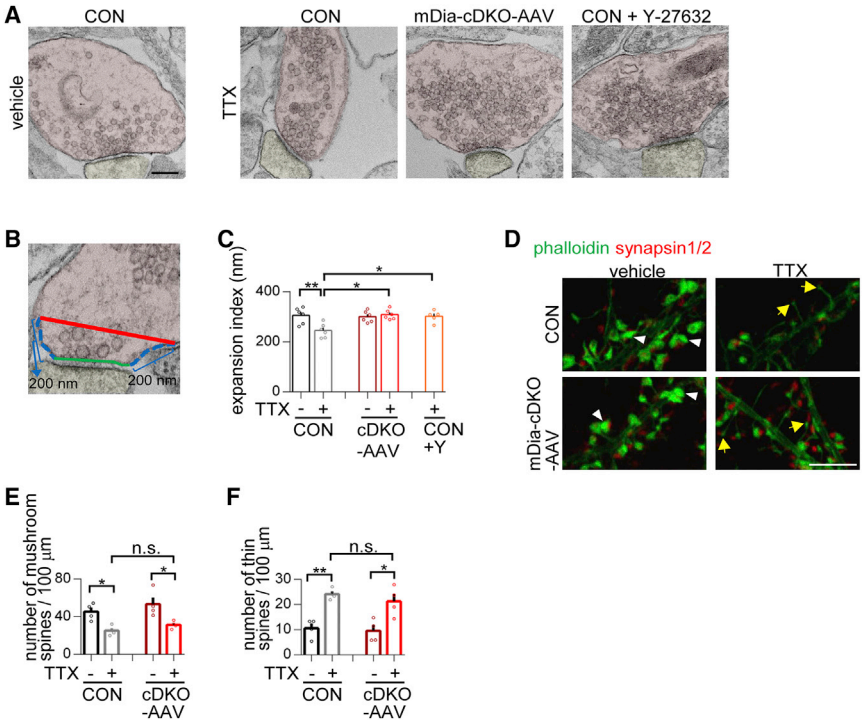

Figure 5. Inactivation-Induced, mDia-Dependent Presynaptic Contraction of Asymmetric Synapses in Cultured Neurons

(A–C) Representative electron micrographs of asymmetric synapses of TTX-treated control (CON), mDia-cDKO-AAV, and control neurons simultaneously treated with Y-27632 (CON+Y-27632) (A) and their expansion index (B and C). (A) Presynaptic or postsynaptic structures are colored in pale red or yellow, respectively. Scale bar, 200 nm. (B) The expansion index is defined as the difference between the length of a synaptic cleft (green line) and the breadth of the presynaptic terminal at 200 nm (red line) along the membranes from both ends of synaptic cleft (blue dotted line). (C) The expansion index of asymmetric synapses in indicated conditions. n = 5–6 independent cultures (10–17 synapses per culture) for respective groups. $^{**}p < 0.01$ and $^{*}p < 0.05$, Bonferroni post hoc test following one-way ANOVA. (C) Data are shown as mean ± SEM.

(D) Representative images of phalloidin staining (green) and staining for synapsin1/2 (red). White arrowheads or yellow arrows indicate mushroom or thin spines, respectively. Scale bar, 5 μm.

(E and F) Densities of mushroom (E) and thin spines (F) along dendrites. n = 4 independent cultures (63–631 spines per culture) for each group. $^{*}p < 0.05$, $^{**}p < 0.01$, and not significant (n.s.), Bonferroni post hoc test following two-way ANOVA. Data are shown as mean ± SEM.

See also Figure S5.

We also analyzed the morphological change of asymmetric, putative excitatory presynapses on the dendritic spines. TTX treatment for 24 hr also induced contraction of these asymmetric presynapses in TTX-treated control neurons. This TTX-induced presynaptic contraction occurred in neither mDia-cDKO-AAV neurons nor Y-27632-treated control neurons (Figures 5A–5C and S5I). Notably, synaptic vesicles tended to stay closer to the active zone in the presynaptic terminal, especially with shorter synaptic clefts of mDia-deficient neurons, compared with control neurons after TTX treatment (Figure S5J), whereas similar numbers of mitochondria and dense core vesicles were found in the presynaptic terminals of mDia-cDKO-AAV neurons and control neurons (Figure S5K).

Taken together, prolonged neuronal inactivation induces presynaptic contraction in both inhibitory and excitatory synapses through mDia. In contrast, whereas the prolonged TTX treatment also induced morphological changes in dendritic spines such as decrease in mushroom spines and increase in thin spines, mDia appears not to be involved in these postsynaptic changes (Figures 5D–5F).

Social Isolation Induces Presynaptic Contraction of NAc Neurons in an mDia/ROCK-Dependent Manner

Given that neuronal inactivation induced mDia- and ROCK-dependent presynaptic contraction in cultured neurons, we examined whether similar presynaptic remodeling by mDia and ROCK occurs in NAc neurons of mice subjected to social isolation. We visualized projections from the NAc of mDiaDF mice by injecting AAV-mCherry into the NAc, and deleted mDia by simultaneous injection of AAV-Cre into the NAc (mDia-cDKO-NAc) (Figure 6A). Because mDia1 and mDia3 of NAc neurons were involved in sensitization to repeated cocaine exposure of NAc projection to the VTA (Figure S2D), we analyzed mCherry-positive GABAergic presynaptic terminals of NAc neurons in the VTA by immunoelectron microscopy (Figure 6B). Without social isolation, the length of the synaptic cleft of these terminals appeared not to be different between control and mDia-cDKO-NAc mice (Figures 6C and S6A). In contrast, social isolation induced shortening of the synaptic cleft length of these GABAergic terminals in the VTA of control mice, whereas no such shortening occurred in mDia-cDKO-NAc terminals (Figures 6C and S6A). This social-isolation-induced shortening of the synaptic cleft length in control mice was more evident for its shorter segment than its longer segment (Figures S6B and S6C). We then injected Y-27632 into the VTA of mice subjected to social isolation and examined whether ROCK inhibition in situ attenuates presynaptic contraction of NAc neurons (Figure 6D). The Y-27632 injection significantly extended the synaptic cleft length of mCherry-positive presynaptic terminals of NAc neurons compared with the vehicle artificial cerebrospinal fluid (aCSF)-injected group (Figures 6E, 6F, and S6D). On the other hand, the length of PSD of these synapses was not significantly altered by social isolation in control mice, mDia-cDKO-NAc mice, or Y-27632-injected mice (Figures 6F and S6E). On light microscopy, social isolation apparently induced mCherry-positive presynaptic terminals of compact round shape in the VTA of control mice, whereas torus-shaped presynaptic terminals were more frequently seen in the VTA of mDia-cDKO-NAc mice (Figure S6F). These findings suggest that social isolation induces presynaptic contraction through mDia and ROCK at GABAergic terminals from the NAc to the VTA.

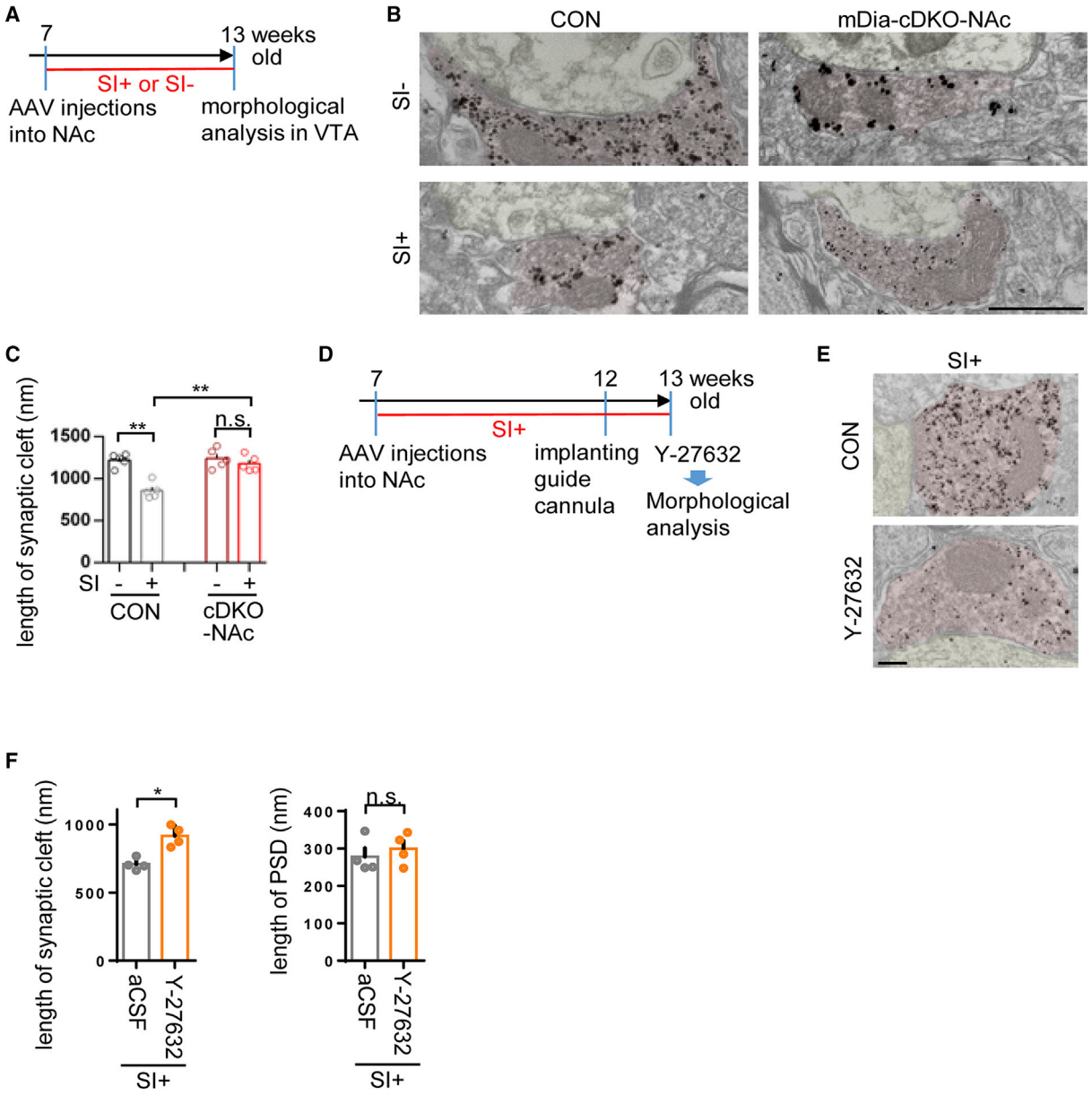

Figure 6. Social-Isolation-Induced, mDia- and ROCK-Dependent Presynaptic Contraction of GABAergic Terminals of NAc Neurons in the VTA

(A) Protocol for morphological analysis.

(B and C) Representative silver-enhanced immunogold electron micrographs for mCherry and the synaptic cleft length of synapses from NAc neurons to the VTA of control and mDia-cDKO-NAc mice with or without social isolation (SI). (B) Synapses identified as mCherry-positive presynaptic terminals from the NAc (red) juxtaposed with mCherry-negative dendritic shafts of VTA neurons (yellow) are shown. Scale bar, 500 nm. (C) Only the synapses with PSD longer than 150 nm were analyzed. n = 5 mice (8–20 synapses per mouse) for each group. **$p < 0.01$ and not significant (n.s.), Bonferroni post hoc test following two-way ANOVA. (C) Data are shown as mean ± SEM.

(D) Protocol for Y-27632 injection for morphological analysis.

(E and F) Representative silver-enhanced immunogold electron micrographs for mCherry (E) and the synaptic cleft (left) and PSD (right) length (F) of synapses from NAc neurons to the VTA of aCSF- (control) and Y-27632-injected mice. Scale bar, 200 nm. n = 4 mice (12–18 synapses per mouse) for each group in (F). *$p < 0.05$ and not significant (n.s.), Mann-Whitney test. (F) Data are shown as mean ± SEM.

See also Figure S6.

Social Isolation Reduced Synaptic Efficacy in an mDia-Dependent Manner

GABAergic projections of NAc neurons primarily form synapses onto GABAergic neurons in the VTA (Xia et al., 2011; Bocklisch et al., 2013). Therefore, we analyzed the effect of social isolation on IPSCs derived from GABAergic synapses from NAc neurons to tyrosine hydroxylase (TH)-negative VTA neurons and a role of mDia therein (Figure S7A). We introduced the

H134R form of channel rhodopsin-2 (ChR2-H134R) in NAc neurons by AAV, prepared acute slices, and stimulated their axon terminals in the VTA with one 0.5-ms blue light pulse (Figure 7A). Optogenetic stimulation evoked IPSCs (eIPSCs) in TH-negative neurons at a short latency (Figure S7B). These eIPSCs were sensitive to picrotoxin, a $GABA_A$ receptor blocker, indicating these neurons directly receive GABAergic projection from NAc neurons (Figure S7B). We then examined the amplitudes of spontaneous IPSCs (sIPSCs) in these light-responsive neurons and found that those in mDia-cDKO-NAc mice were larger than those of control mice similarly subjected to social isolation (Figures S7C and S7D). Neither mDia deficiency nor social isolation significantly affected the frequencies of sIPSCs (Figure S7E).

We next analyzed effects of social isolation on eIPSCs from TH-negative VTA neurons. Neither social isolation nor mDia deficiency significantly affected the amplitudes of eIPSCs evoked by a single light pulse of the same intensity (Figure S7F). To analyze presynaptic functions, we measured the paired-pulse ratio (PPR) of these eIPSCs. The GABAergic synapses of non-isolated control mice showed paired-pulse depression, a depression of eIPSCs on the second pulse applied at 50-ms intervals (Figures 7B, 7C, and S7G). Social isolation induced a significantly larger PPR in control mice, whereas the PPR in mDia-cDKO-NAc mice subjected to social isolation remained small (Figures 7B, 7C, and S7G). As observed in paired-pulse analysis by electronic stimulation, paired-pulse depression induced by optogenetic stimulation was reduced by increasing the interval of the paired pulses (Figure S7H). These results suggest that social isolation decreases the release probability of GABAergic synaptic vesicles at presynaptic terminals from NAc neurons on TH-negative VTA neurons, and that mDia1 and mDia3 play a critical role in induction of this suppression.

GABAergic transmission is determined not only by its release probability, but also its uptake. GABA is taken up by astrocytes through GABA transporter (GAT) 3, which promotes termination of GABAergic transmission and reduces a half decay of IPSCs (Jin et al., 2011). GAT3 is present at processes of astrocytes localized adjacent to GABAergic synapses. Because social isolation reduced the length of synaptic cleft of NAc-derived GABAergic synapses in the VTA, we hypothesized that astrocytic GAT3 is more accessible to GABA released to the synaptic cleft after social isolation. To explore this possibility, we examined the contribution of GAT3-mediated GABA uptake by bath application of SNAP5114, a GAT2/3-selective blocker (Figure 7D). SNAP5114 is used as a GAT3 blocker in studies of the central nervous system because GAT3 is much more abundant than GAT2 in the brain. SNAP5114 treatment extended the half decay of NAc-derived eIPSCs upon optogenetic stimulation in TH-negative VTA neurons of isolated control mice, and this effect was attenuated by mDia deficiency (Figures 7D and 7E). Neither mDia deficiency nor SNAP5114 treatment affected the onset and rise time of eIPSCs obtained from isolated mice (Figures S7I and S7J). These findings suggest that GAT3-mediated GABA uptake is involved in social-isolation-induced, mDia-dependent attenuation of synaptic efficacy at GABAergic synapses from NAc to VTA neurons.

Optogenetic Stimulation of NAc Neurons and Injection of Y-27632 into the VTA Rescued the Social-Isolation-Induced Anxiety-like Phenotype

Finally, we examined whether the earlier mDia-dependent attenuation of synaptic transmission contributed to induction of anxiety-like behavior by social isolation and whether the mDia- and ROCK-dependent presynaptic contraction is involved in this process. To address the former, we attempted to rescue the behavioral phenotype by stimulating NAc neurons. A fusion protein of channelrhodopsin-2 (ChR2) and EGFP (ChR2-EGFP) was expressed in NAc neurons by AAV. Using patch-clamp recording with acute NAc slices, we confirmed that a 50-Hz train of 3-ms blue light pulses reproducibly evoked action potentials in NAc neurons expressing ChR2-EGFP (Figures 7F and 7G). Repeated cycles of the same pattern of light stimulation for 5 s followed by 15 s of rest were delivered to the NAc through optogenetic probes during the first 5 min of EPM test (on) and then no light stimulation during next 5 min (off). Notably, the optogenetic stimulation significantly suppressed social-isolation-induced, anxiety-like behaviors in EPM of mDia-intact mice (Figure 7H). To address the ROCK involvement, we injected Y-27632 or aCSF into both sides of the VTA through a thin glass capillary 24 hr before EPM (Figure S7K). The Y-27632 injection significantly attenuated social-isolation-induced, anxiety-like behavior in EPM (Figure 7I), whereas the moving distance during EPM was not significantly different between Y-27632- and aCSF-injected groups (Figure 7I). These results indicate that the social-isolation-induced, mDia- and ROCK-dependent presynaptic contraction and attenuated synaptic transmission of NAc neurons underlie the elevated anxiety-like behavior.

DISCUSSION

Compared with postsynaptic effects, little is known about presynaptic remodeling in matured brains and its behavioral relevance. Here we examined this issue by analyzing the action of mDia. Our findings are as follows. In cultured neurons, neuronal inactivation recruits mDia to the presynapse, which induces circumferential actin filaments at the edge of the synaptic cleft and contracts the presynaptic terminals with ROCK and myosin. In adult mice, prolonged social isolation induces mDia-dependent presynaptic contraction of GABAergic synapses from NAc neurons in the VTA and reduction of synaptic efficacy characterized by decreased release probability and enhanced sensitivity to astrocyte GAT3, which is associated with elevated anxiety-like behavior. The presynaptic contraction and anxiety-like behavior are reversed by injection of a ROCK inhibitor to the VTA. Based on these findings, we propose the mode of mDia- and ROCK-dependent presynaptic remodeling as depicted in Figure S7L.

mDia Mediates Behavioral Plasticity in Adult Mice

mDia in NAc neurons is thus critical for isolation-induced elevated anxiety. Reversal of this phenotype by optogenetic stimulation suggests that mDia-mediated attenuation of GABAergic transmission from NAc neurons to the VTA is responsible for the elevated anxiety. This mDia action is also supported by the mDia-dependent attenuation of cocaine-induced behavioral sensitization, which is mediated by plasticity of synapses from

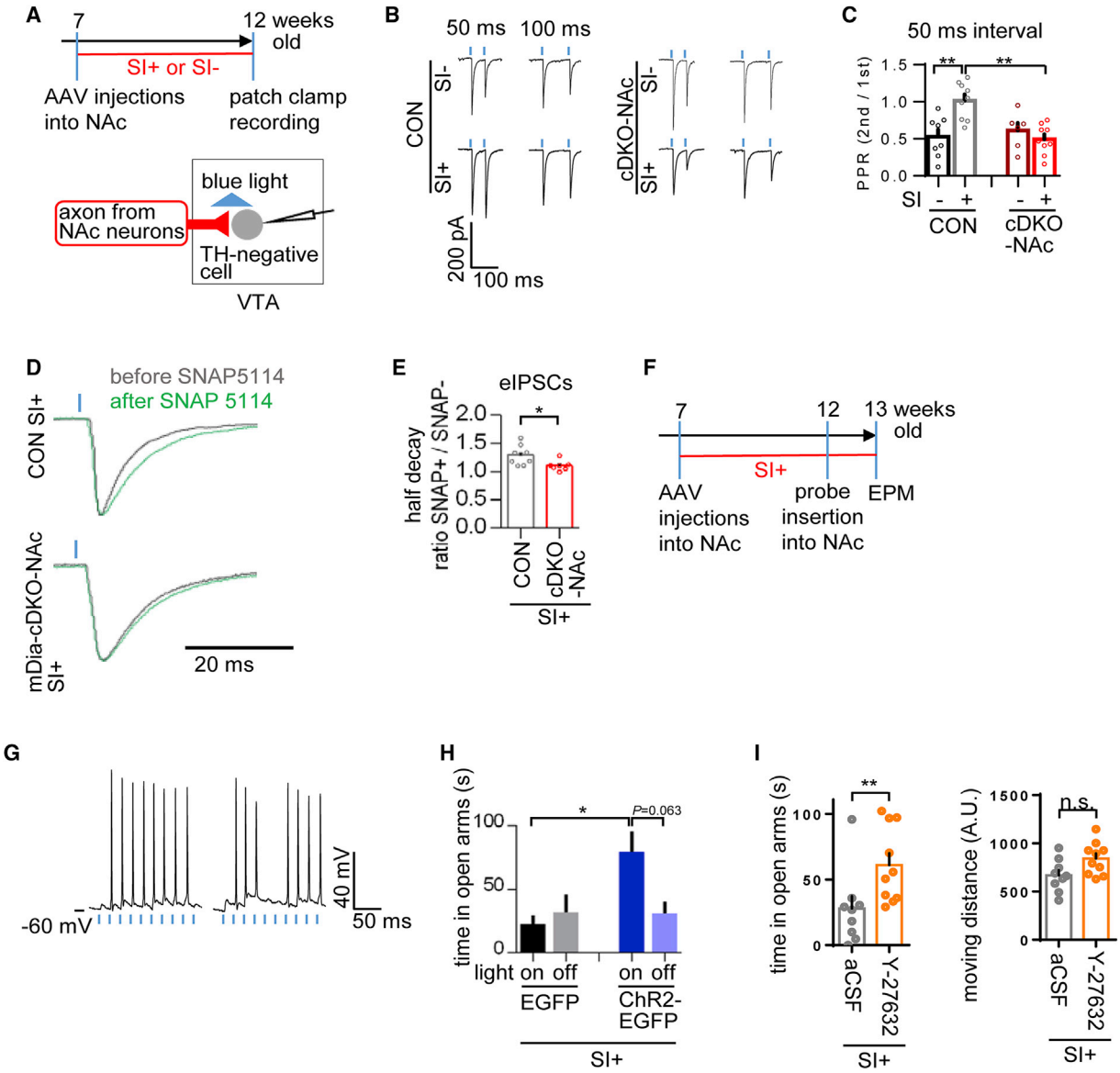

Figure 7. Reduced Synaptic Efficacy of GABAergic Synapses in the VTA after Social Isolation and Phenotype Reversal by Optogenetic Stimulation and Y-27632 Injection

(A) Protocol for activity measurement of NAc neuron synapses to TH-negative VTA neurons with optogenetic stimulations.

(B) Representative traces of eIPSCs upon paired light stimulations (blue bars) with 50 or 100 ms intervals.

(C) PPR with 50 ms intervals of control and mDia-cDKO-NAc mice. n = 6–9 neurons (from 6–8 mice) for respective groups, respectively. **$p < 0.01$, *$p < 0.05$, Bonferroni's post hoc test following two-way ANOVA. Data are shown as mean ± SEM.

(D) Representative averaged traces of eIPSCs before (gray) and after (green) the SNAP5114 treatment. The peak amplitudes of eIPSCs before and after the SNAP addition were normalized.

(E) The ratio of the half decay time for eIPSCs before and after SNAP treatment in indicated mice. n = 9 and 7 neurons (from eight and six mice) for respective groups. *$p < 0.05$, Mann-Whitney test. Data are shown as mean ± SEM.

(F) Protocol for behavioral experiments with optogenetic stimulation of NAc neurons.

(G) Whole-cell current-clamp recording from ChR2-expressing NAc neurons upon 50 Hz light stimulation (blue bars).

(H) Anxiolytic effect of optogenetic stimulation of NAc neurons on EPM after social isolation. n = 7 or 9 for mice expressing EGFP or ChR2-GFP, respectively. Data are shown as mean ± SEM. *$p < 0.05$, Bonferroni's post hoc test following two-way ANOVA. Data are shown as mean ± SEM.

(I) Time in open arms (left) and moving distance (right) during EPM of aCSF- and Y-27632-injected mice. n = 9 and 10 mice for each group. **$p < 0.01$ and not significant (n.s.), Mann-Whitney test. Data are shown as mean ± SEM.

See also Figure S7.

NAc neurons to the VTA. mDia in NAc neurons is also critical for isolation-induced decrease in CREB phosphorylation in the whole population of NAc neurons. This phenotype indicates that, once some population of NAc neurons is inactivated by isolation, mDia induces presynaptic contraction of these neurons and reduces GABAergic inputs from these NAc neurons to VTA GABAergic neurons, resulting in decreased dopaminergic inputs to the NAc. This idea can explain that the decrease in CREB phosphorylation was attenuated in both mDia-deleted and mDia-intact neurons, although other mechanisms may also exist.

Our findings that suppression of the GABAergic projection from NAc neurons to the VTA enhances anxiety indicate that this pathway can be an action site of anxiolytic drugs, although GABAergic neurotransmission in the amygdala is thought as their primary action site (Nuss, 2015). Our suggestion is supported by several studies such as the association of reduced dopamine release with anxiety in Parkinson's disease patients (Beitz, 2014), increased firing of VTA dopamine neurons by benzodiazepines through inhibition of VTA GABAergic neurons (Tan et al., 2010), and reduction of social-isolation-induced, anxiety-like behavior by an acute administration of diazepam to adult rats (Simpson and Kelly, 2012).

Intriguingly, mDia regulates anxiety in a context-dependent manner; anxiety induced by social isolation is dependent on mDia, but not that induced by chronic social defeat stress. Stress can be classified into two categories: one is "active stress," such as social defeat and foot shock that are accompanied by pain and fear; and another is "passive stress," such as social isolation that is not accompanied by pain (Wallace et al., 2009). Whereas both stresses induce anxiety-like behavior in mice, the states of CREB activity in NAc neurons exhibit opposite responses: activation to social defeat and inactivation to social isolation (Wilkinson et al., 2009). These results are consistent with our finding that mDia signaling is activated by neuronal inactivation and not by activation.

In addition to altered anxiety-like behavior after social isolation, mDia-cDKO-Wfs1 mice showed better performance in the radial maze task. The site and manner of mDia action in this phenotype remains to be elucidated.

Presynaptic Remodeling and Its Consequences

Our study has shown mDia- and ROCK-mediated presynaptic contraction both in cultured neurons and in NAc neurons in vivo. Given the differences in neuronal types and conditions, such similarity is remarkable, suggesting that this is a general adaptation mechanism for neuronal inactivation. Functionally, in cultured neurons, the amplitude of mIPSCs is decreased in an mDia-dependent manner. The amplitude of mIPSCs generally reflects the amount of correspondent receptors available on the postsynaptic membrane. Because the actin cytoskeleton plays a role in receptor trafficking, mDia might be involved in trafficking of postsynaptic receptors. However, another possibility more pertinent to our results is that presynaptic contraction affects the number of GABA receptors available in a GABAergic synapse. Because β2/3 subunits of $GABA_A$ receptors are distributed entirely along the synaptic cleft even outside the PSD (Fujiyama et al., 2000), mDia-mediated presynaptic contraction could decrease the amount of $GABA_A$ receptors facing the presynaptic terminal, thus leading to reduction in mIPSC amplitude. In adult brain, decrease in amplitudes of sIPSCs and release probability of synaptic vesicles and increase in sensitivity to GAT2/3 occur in an mDia-dependent manner. The decrease in the sIPSC amplitude is similar to that found in mIPSCs in cultured neurons, and this similarity may indicate that mDia similarly functions in vitro and in vivo. The decrease in the release probability of synaptic vesicles could be explained by alteration in distribution of synaptic vesicles by presynaptic contraction. Finally, increased sensitivity to GAT2/3 can be due to closer astrocytic processes to the GABA release site by presynaptic contraction, given that the distance between PSD and astrocytic processes was critical for the efficacy of glutamate uptake (Pannasch et al., 2014) and given the mDia-mediated shortening of the length of synaptic clefts.

Possible Molecular Machineries Regulating mDia at Presynaptic Terminals

There remain a few questions. One question is how the above mechanism is triggered. Our findings on mDia localization suggest that there is a molecular mechanism to recruit mDia into presynaptic terminals upon neuronal inactivation. Because mDia and ROCK are Rho effectors and Rho activation regulates localization of mDia in non-neuronal cells (Watanabe et al., 2010), Rho activation conceivably precedes mDia accumulation in the presynaptic terminal. Little is known on activation mechanism of Rho upon neuronal inactivation. The Wnt-disheveled signaling that regulates presynaptic morphology and synapse numbers in the hippocampus in an enriched environment (Gogolla et al., 2009) is known to activate Rho upon neuronal activation, but not inactivation (Budnik and Salinas, 2011). In addition to Rho, mDia may also require other binding partners to elicit its action in the presynaptic terminal. One candidate is liprin α, which regulates localization of mDia in non-neuronal cells (Sakamoto et al., 2012). Liprin α is enriched in the active zone of presynaptic terminals and is critical for maintaining it (Stryker and Johnson, 2007). Similar targeting of a formin protein to the active zone for actin assembly was reported between piccolo and Daam1 (Wagh et al., 2015). Another question is whether mDia activated in the presynaptic terminals regulates cell adhesion at the synapse. The region surrounding the active zone toward the edge of the synaptic cleft is the site for cell adhesion between presynaptic and postsynaptic membrane (Takai et al., 2003). In non-neuronal cells, the cell-cell adhesion is regulated by Rho GTPases (Parsons et al., 2010), and mDia is one of the players (Carramusa et al., 2007).

Here we have identified mDia- and ROCK-mediated presynaptic contraction as a presynaptic mechanism for synaptic and behavioral plasticity in mammals. Although our current analysis was focused on the GABAergic presynaptic terminals in VTA of the adult brain and anxiety-like behavior, this activity-dependent presynaptic morphological remodeling may also operate in other neuronal systems to link synaptic plasticity to animal behaviors.

EXPERIMENTAL PROCEDURES

Animals

mDia1-floxed mice (accession number CDB0437K) and *mDia3*-floxed mice (accession number CDB0426K) were generated and backcrossed to

C57BL/6NCrSlc mice for more than 10 generations (see the Supplemental Experimental Procedures for details).

Construction and Production of AAVs

Detailed procedures of the production of AAVs are described in the Supplemental Experimental Procedures.

Stereotaxic Injection of AAV

Stereotaxic injection into the NAc was performed as previously described (Tanaka et al., 2012) according to a mouse brain atlas (see Supplemental Experimental Procedures).

Behavioral Experiments

Social isolation was applied as previously described with modifications (Conrad et al., 2011). Repeated social defeat stress, social interaction test, and the elevated plus maze were performed as described previously with minor modifications (Tanaka et al., 2012) (see Supplemental Experimental Procedures).

Optogenetic Stimulation during the Behavioral Test

For optogenetic stimulations during the behavior test, detailed procedures are described in the Supplemental Experimental Procedures.

Primary Culture of Hippocampal Neurons Followed by AAV Infection

Detailed procedures of preparation for primary hippocampal neurons are described in the Supplemental Experimental Procedures.

Electron Microscopy

For immunoelectron or electron microscopy with brain specimens or cultured primary neurons, detailed procedures are described in the Supplemental Experimental Procedures.

Slice Preparation and Electrophysiology

Whole-cell recording was performed as described previously with modifications (Bocklisch et al., 2013) (see the Supplemental Experimental Procedures).

Immunofluorescence Staining

Immunofluorescence staining was performed as described previously with minor modifications (Shinohara et al., 2012) (see the Supplemental Experimental Procedures).

Statistical Analysis

All data in bar graphs are shown as means ± SEM unless stated otherwise. Comparison of two groups was analyzed using the Mann-Whitney test. For comparison of more than two groups, one-way or two-way ANOVA was performed and followed by Bonferroni post hoc test for evaluation of pairwise group differences. For comparison of paired test, Wilcoxon matched-pairs signed rank test was performed. A p value less than 0.05 was considered statistically significant. Prism 6.0 software (GraphPad) was used for the analysis.

SUPPLEMENTAL INFORMATION

Supplemental Information includes Supplemental Experimental Procedures and seven figures and can be found with this article online at http://dx.doi.org/10.1016/j.celrep.2016.10.088.

AUTHOR CONTRIBUTIONS

S.N., T.F., and Y.D. conceived the idea, designed experiments, and wrote the manuscript. Y.D., M.H., and R.S. performed experiments and analyzed data. D.W., M.S., and D.Y. contributed to electrophysiology experiments. Y.U., M.L., and Y.C. contributed to AAV experiments.

ACKNOWLEDGMENTS

We thank K. Furuta and H. Kohda for electron microscope photograph. This study was supported by Grants-in-Aid for Scientific Research from the Ministry of Education, Culture, Sports, Science and Technology of Japan (grants 26221302 to S.N. and 24689015 to T.F.). Y.D. and R.S. were postdoctoral fellows of the Japan Society for Promotion of Science.

Received: March 20, 2015
Revised: September 26, 2016
Accepted: October 28, 2016
Published: November 22, 2016

REFERENCES

Beitz, J.M. (2014). Parkinson's disease: a review. Front. Biosci. (Schol. Ed.) *6*, 65–74.

Bleckert, A., Photowala, H., and Alford, S. (2012). Dual pools of actin at presynaptic terminals. J. Neurophysiol. *107*, 3479–3492.

Bocklisch, C., Pascoli, V., Wong, J.C., House, D.R., Yvon, C., de Roo, M., Tan, K.R., and Lüscher, C. (2013). Cocaine disinhibits dopamine neurons by potentiation of GABA transmission in the ventral tegmental area. Science *341*, 1521–1525.

Bosch, M., and Hayashi, Y. (2012). Structural plasticity of dendritic spines. Curr. Opin. Neurobiol. *22*, 383–388.

Budnik, V., and Salinas, P.C. (2011). Wnt signaling during synaptic development and plasticity. Curr. Opin. Neurobiol. *21*, 151–159.

Burkel, B.M., von Dassow, G., and Bement, W.M. (2007). Versatile fluorescent probes for actin filaments based on the actin-binding domain of utrophin. Cell Motil. Cytoskeleton *64*, 822–832.

Caroni, P., Donato, F., and Muller, D. (2012). Structural plasticity upon learning: regulation and functions. Nat. Rev. Neurosci. *13*, 478–490.

Carramusa, L., Ballestrem, C., Zilberman, Y., and Bershadsky, A.D. (2007). Mammalian diaphanous-related formin Dia1 controls the organization of E-cadherin-mediated cell-cell junctions. J. Cell Sci. *120*, 3870–3882.

Conrad, K.L., Louderback, K.M., Gessner, C.P., and Winder, D.G. (2011). Stress-induced alterations in anxiety-like behavior and adaptations in plasticity in the bed nucleus of the stria terminalis. Physiol. Behav. *104*, 248–256.

De Filippis, B., Romano, E., and Laviola, G. (2014). Aberrant Rho GTPases signaling and cognitive dysfunction: in vivo evidence for a compelling molecular relationship. Neurosci. Biobehav. Rev. *46*, 285–301.

Fujiyama, F., Fritschy, J.M., Stephenson, F.A., and Bolam, J.P. (2000). Synaptic localization of GABA(A) receptor subunits in the striatum of the rat. J. Comp. Neurol. *416*, 158–172.

Gogolla, N., Galimberti, I., Deguchi, Y., and Caroni, P. (2009). Wnt signaling mediates experience-related regulation of synapse numbers and mossy fiber connectivities in the adult hippocampus. Neuron *62*, 510–525.

Golden, S.A., Christoffel, D.J., Heshmati, M., Hodes, G.E., Magida, J., Davis, K., Cahill, M.E., Dias, C., Ribeiro, E., Ables, J.L., et al. (2013). Epigenetic regulation of RAC1 induces synaptic remodeling in stress disorders and depression. Nat. Med. *19*, 337–344.

Hall, A., and Nobes, C.D. (2000). Rho GTPases: molecular switches that control the organization and dynamics of the actin cytoskeleton. Philos. Trans. R. Soc. Lond. B Biol. Sci. *355*, 965–970.

Jin, X.T., Galvan, A., Wichmann, T., and Smith, Y. (2011). Localization and function of GABA transporters GAT-1 and GAT-3 in the basal ganglia. Front. Syst. Neurosci. *5*, 63.

Madisen, L., Mao, T., Koch, H., Zhuo, J.M., Berenyi, A., Fujisawa, S., Hsu, Y.W., Garcia, A.J., 3rd, Gu, X., Zanella, S., et al. (2012). A toolbox of Cre-dependent optogenetic transgenic mice for light-induced activation and silencing. Nat. Neurosci. *15*, 793–802.

Morales, M., Colicos, M.A., and Goda, Y. (2000). Actin-dependent regulation of neurotransmitter release at central synapses. Neuron *27*, 539–550.

Narumiya, S., Tanji, M., and Ishizaki, T. (2009). Rho signaling, ROCK and mDia1, in transformation, metastasis and invasion. Cancer Metastasis Rev. *28*, 65–76.

Nuss, P. (2015). Anxiety disorders and GABA neurotransmission: a disturbance of modulation. Neuropsychiatr. Dis. Treat. *11*, 165–175.

Pannasch, U., Freche, D., Dallérac, G., Ghézali, G., Escartin, C., Ezan, P., Cohen-Salmon, M., Benchenane, K., Abudara, V., Dufour, A., et al. (2014). Connexin 30 sets synaptic strength by controlling astroglial synapse invasion. Nat. Neurosci. *17*, 549–558.

Parsons, J.T., Horwitz, A.R., and Schwartz, M.A. (2010). Cell adhesion: integrating cytoskeletal dynamics and cellular tension. Nat. Rev. Mol. Cell Biol. *11*, 633–643.

Pawson, C., Eaton, B.A., and Davis, G.W. (2008). Formin-dependent synaptic growth: evidence that Dlar signals via Diaphanous to modulate synaptic actin and dynamic pioneer microtubules. J. Neurosci. *28*, 11111–11123.

Pilo Boyl, P., Di Nardo, A., Mulle, C., Sassoè-Pognetto, M., Panzanelli, P., Mele, A., Kneussel, M., Costantini, V., Perlas, E., Massimi, M., et al. (2007). Profilin2 contributes to synaptic vesicle exocytosis, neuronal excitability, and novelty-seeking behavior. EMBO J. *26*, 2991–3002.

Sakamoto, S., Ishizaki, T., Okawa, K., Watanabe, S., Arakawa, T., Watanabe, N., and Narumiya, S. (2012). Liprin-α controls stress fiber formation by binding to mDia and regulating its membrane localization. J. Cell Sci. *125*, 108–120.

Sankaranarayanan, S., Atluri, P.P., and Ryan, T.A. (2003). Actin has a molecular scaffolding, not propulsive, role in presynaptic function. Nat. Neurosci. *6*, 127–135.

Shinohara, R., Thumkeo, D., Kamijo, H., Kaneko, N., Sawamoto, K., Watanabe, K., Takebayashi, H., Kiyonari, H., Ishizaki, T., Furuyashiki, T., and Narumiya, S. (2012). A role for mDia, a Rho-regulated actin nucleator, in tangential migration of interneuron precursors. Nat. Neurosci. *15*, 373–380, S1–S2.

Simpson, J., and Kelly, J.P. (2012). The effects of isolated and enriched housing conditions on baseline and drug-induced behavioural responses in the male rat. Behav. Brain Res. *234*, 175–183.

Stryker, E., and Johnson, K.G. (2007). LAR, liprin alpha and the regulation of active zone morphogenesis. J. Cell Sci. *120*, 3723–3728.

Takai, Y., Shimizu, K., and Ohtsuka, T. (2003). The roles of cadherins and nectins in interneuronal synapse formation. Curr. Opin. Neurobiol. *13*, 520–526.

Tan, K.R., Brown, M., Labouèbe, G., Yvon, C., Creton, C., Fritschy, J.M., Rudolph, U., and Lüscher, C. (2010). Neural bases for addictive properties of benzodiazepines. Nature *463*, 769–774.

Tanaka, K., Furuyashiki, T., Kitaoka, S., Senzai, Y., Imoto, Y., Segi-Nishida, E., Deguchi, Y., Breyer, R.M., Breyer, M.D., and Narumiya, S. (2012). Prostaglandin E2-mediated attenuation of mesocortical dopaminergic pathway is critical for susceptibility to repeated social defeat stress in mice. J. Neurosci. *32*, 4319–4329.

Thumkeo, D., Shinohara, R., Watanabe, K., Takebayashi, H., Toyoda, Y., Tohyama, K., Ishizaki, T., Furuyashiki, T., and Narumiya, S. (2011). Deficiency of mDia, an actin nucleator, disrupts integrity of neuroepithelium and causes periventricular dysplasia. PLoS ONE *6*, e25465.

Tolias, K.F., Duman, J.G., and Um, K. (2011). Control of synapse development and plasticity by Rho GTPase regulatory proteins. Prog. Neurobiol. *94*, 133–148.

Wagh, D., Terry-Lorenzo, R., Waites, C.L., Leal-Ortiz, S.A., Maas, C., Reimer, R.J., and Garner, C.C. (2015). Piccolo directs activity dependent F-actin assembly from presynaptic active zones via Daam1. PLoS ONE *10*, e0120093.

Wallace, D.L., Han, M.H., Graham, D.L., Green, T.A., Vialou, V., Iñiguez, S.D., Cao, J.L., Kirk, A., Chakravarty, S., Kumar, A., et al. (2009). CREB regulation of nucleus accumbens excitability mediates social isolation-induced behavioral deficits. Nat. Neurosci. *12*, 200–209.

Watanabe, N., Madaule, P., Reid, T., Ishizaki, T., Watanabe, G., Kakizuka, A., Saito, Y., Nakao, K., Jockusch, B.M., and Narumiya, S. (1997). p140mDia, a mammalian homolog of Drosophila diaphanous, is a target protein for Rho small GTPase and is a ligand for profilin. EMBO J. *16*, 3044–3056.

Watanabe, S., Okawa, K., Miki, T., Sakamoto, S., Morinaga, T., Segawa, K., Arakawa, T., Kinoshita, M., Ishizaki, T., and Narumiya, S. (2010). Rho and anillin-dependent control of mDia2 localization and function in cytokinesis. Mol. Biol. Cell *21*, 3193–3204.

Watanabe, S., Rost, B.R., Camacho-Pérez, M., Davis, M.W., Söhl-Kielczynski, B., Rosenmund, C., and Jorgensen, E.M. (2013). Ultrafast endocytosis at mouse hippocampal synapses. Nature *504*, 242–247.

Wilkinson, M.B., Xiao, G., Kumar, A., LaPlant, Q., Renthal, W., Sikder, D., Kodadek, T.J., and Nestler, E.J. (2009). Imipramine treatment and resiliency exhibit similar chromatin regulation in the mouse nucleus accumbens in depression models. J. Neurosci. *29*, 7820–7832.

Xia, Y., Driscoll, J.R., Wilbrecht, L., Margolis, E.B., Fields, H.L., and Hjelmstad, G.O. (2011). Nucleus accumbens medium spiny neurons target non-dopaminergic neurons in the ventral tegmental area. J. Neurosci. *31*, 7811–7816.

Xu, T., Yu, X., Perlik, A.J., Tobin, W.F., Zweig, J.A., Tennant, K., Jones, T., and Zuo, Y. (2009). Rapid formation and selective stabilization of synapses for enduring motor memories. Nature *462*, 915–919.